# Intracalibration of particle detectors on a three-axis stabilized geostationary platform

W. Rowland[1,2,3,4,5] and R. S. Weigel[3]

Received 22 May 2012; revised 27 September 2012; accepted 1 October 2012; published 21 November 2012.

[1] We describe an algorithm for intracalibration of measurements from plasma or energetic particle detectors on a three-axis stabilized platform. Modeling and forecasting of Earth's radiation belt environment requires data from particle instruments, and these data depend on measurements which have an inherent calibration uncertainty. Pre-launch calibration is typically performed, but on-orbit changes in the instrument often necessitate adjustment of calibration parameters to mitigate the effect of these changes on the measurements. On-orbit calibration practices for particle detectors aboard spin-stabilized spacecraft are well established. Three-axis stabilized platforms, however, pose unique challenges even when comparisons are being performed between multiple telescopes measuring the same energy ranges aboard the same satellite. This algorithm identifies time intervals when different telescopes are measuring particles with the same pitch angles. These measurements are used to compute scale factors which can be multiplied by the pre-launch geometric factor to correct any changes. The approach is first tested using measurements from GOES-13 MAGED particle detectors over a 5-month time period in 2010. We find statistically significant variations which are generally on the order of 5% or less. These results do not appear to be dependent on Poisson statistics nor upon whether a dead time correction was performed. When applied to data from a 5-month interval in 2011, one telescope shows a 10% shift from the 2010 scale factors. This technique has potential for operational use to help maintain relative calibration between multiple telescopes aboard a single satellite. It should also be extensible to inter-calibration between multiple satellites.

**Citation:** Rowland, W., and R. S. Weigel (2012), Intracalibration of particle detectors on a three-axis stabilized geostationary platform, *Space Weather*, *10*, S11002, doi:10.1029/2012SW000816.

## 1. Introduction

[2] Several techniques can be used for on-orbit calibration of particle detectors. The appropriate technique depends upon the specifics of the instrument and satellite, such as whether or not the satellite is spin-stabilized. Particle detectors on spinning satellites, such as the SOPA instrument aboard LANL satellites, generally sample particles with a range of pitch angles over a short amount of time (10 s spin period about nadir, with 4 samples per second) (http://www.lanl-epdata.lanl.gov/psm/dickb.html). In these cases telescopes aboard a given satellite can sample a wide range of pitch angles during a given 10 s rotation of the satellite, which can simplify the process of calibration. The average over an extended period of time can include measurements from the full range of the particle distribution. Calibration and inter-calibration practices for these telescopes are well established [*Chen et al.*, 2005; *Friedel et al.*, 2005].

[3] Practices for calibration of instruments aboard three-axis-stabilized satellites such as GOES-8 and later are not as well established. Intracalibration of these instruments requires accounting for the fact that each telescope typically samples particles from a different portion of the particle distribution function in a short time interval. In fact, it is possible that two telescopes will never sample particles with the same pitch angle for an extended period of time. For this reason, an attempt to intracalibrate an

[1]Now at Solar Terrestrial Physics Division, National Geophysical Data Center, National Oceanic and Atmospheric Administration, Boulder, Colorado, USA.
[2]Cooperative Institute for Research in the Atmosphere, University of Colorado Boulder, Boulder, Colorado, USA.
[3]School of Physics, Astronomy, and Computational Sciences, George Mason University, Fairfax, Virginia, USA.
[4]Center for Satellite Applications and Research, National Environmental Satellite, Data, and Information Service, National Oceanic and Atmospheric Administration, Camp Springs, Maryland, USA.
[5]IM Systems Group, Rockville, Maryland, USA.

Corresponding author: W. Rowland, Solar Terrestrial Physics Division, National Geophysical Data Center, National Oceanic and Atmospheric Administration, 325 Broadway, Boulder, CO 80305, USA. (william.rowland@noaa.gov)

**Table 1.** MAGED Detector Energy Range[a]

| Channel | Range (keV) | Sample Time (sec) |
|---|---|---|
| ME1 | 30–50 | 2.048 |
| ME2 | 50–100 | 2.048 |
| ME3 | 100–200 | 4.096 |
| ME4 | 200–350 | 16.384 |
| ME5 | 350–600 | 32.768 |

[a]Instrument energy ranges (GOES-N Data Book, 2005, http://goes.gsfc.nasa.gov/text/GOES-N_Databook/databook.pdf).

instrument by a simple comparison of the average fluxes or count rates for two such telescopes can yield very poor results.

[4] Because GOES satellites have on-board magnetometers, it is possible to use the magnetic field measurements to estimate of the pitch angle of particles entering each telescope during its integration cycle. This permits identification of time periods in which one or more telescopes actually are sampling particles with comparable pitch angles. During such times the measured particles should be from the same portion of the distribution function and are therefore expected to have comparable fluxes. Once identified, these data can be collected and used to determine the relative responses of the telescopes. This forms the foundation of the intracalibration procedure tested in this work.

## 2. Instrument and Data

[5] The data initially used for this analysis are from GOES-13 and span a time period from May 4 through September 30 of 2010 (http://satdat.ngdc.noaa.gov/sem/goes/data/new_full/2010). The GOES MAGnetospheric Electron Detector (MAGED) measures electrons in the energy range between 30 keV and 600 keV in 5 discrete energy bands (Table 1). The integration (sample) time of these telescopes ranges from 2.0 s for the lowest energy channels to 32.8 s for the highest energy channel. The instrument consists of nine telescopes, each of which consists of a single Solid State Detector (SSD). The field of view for each telescope is 30 degrees, and a layer of Nickel foil across the aperture blocks contamination from photons. Details of the mechanical configuration of the instrument are recorded in GOESN-ENG-048 (e.g., section 4.2 and Figure 4–3). Table 2 shows that the telescopes are oriented in 35-degree increments, with the central telescope (telescope 1) facing in the zenith direction, two telescopes at +/−35 degrees from zenith in the X-Z and Y-Z planes, and two telescopes at +/−70 degrees from the zenith in the X-Z and Y-Z planes. Figure 1 shows the nominal orientation of each telescope's field of view relative to the Earth when the satellite is in its normal operational configuration. It should be noted that because the measurements which were used for both the particle detectors and the magnetometer are in the body reference

**Table 2.** MAGED Telescope Look Directions[a]

| Telescope Number | FOV Angle to −Z Axis | FOV in +X or +Y Direction | Equatorial/ Polar View |
|---|---|---|---|
| 1 | 0° | - | Anti-earthward/center |
| 2 | 35° | +X | Equatorial/west |
| 3 | 70° | −X | Equatorial/east |
| 4 | 35° | −X | Equatorial/east |
| 5 | 70° | +X | Equatorial/west |
| 6 | 35° | +Y | Polar/north |
| 7 | 70° | −Y | Polar/south |
| 8 | 35° | −Y | Polar/south |
| 9 | 70° | +Y | Polar/north |

[a]GOESN-ENG-048, 2011, http://www.ngdc.noaa.gov/stp/satellite/goes/doc/goes_nop/GOESN-ENG-048_RevD_EPS_HEPAD_13May2011.pdf.

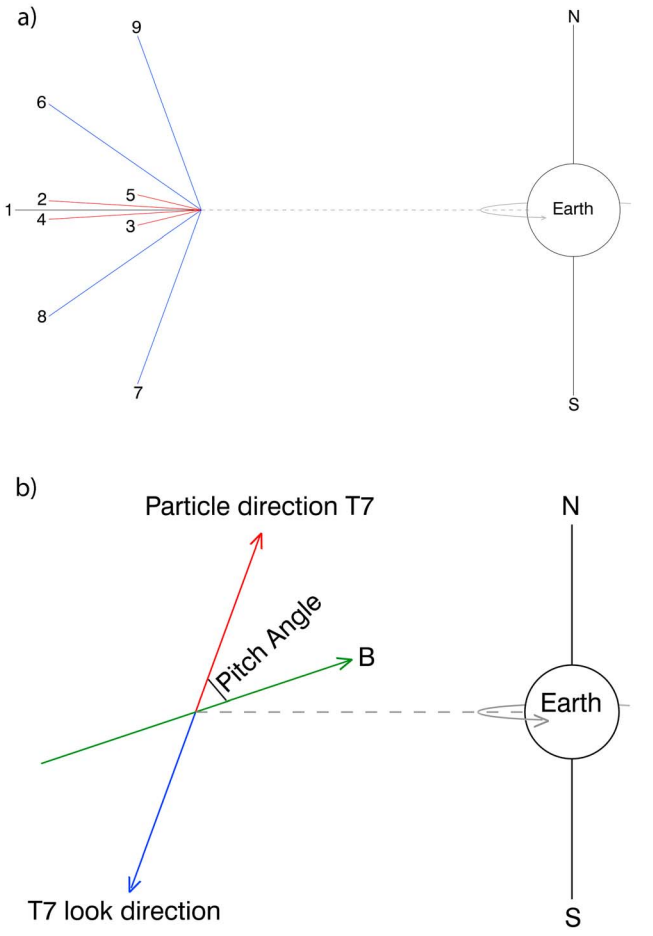


**Figure 1.** Illustration of the GOES-NOP particle detectors. (a.) Telescope nominal pointing directions by telescope number. Telescope 1 points toward zenith. Telescopes 6 through 9 are in the plane of the page, providing coverage from North to South. Telescopes 2 through 5 are in the plane perpendicular to the N-S axis, covering look directions from East to West. The spacing is described in Table 2 (based on information from GOESN-ENG-048, 2011, http://www.ngdc.noaa.gov/stp/satellite/goes/doc/goes_nop/GOESN-ENG-048_RevD_EPS_HEPAD_13May2011.pdf). (b) Illustration of pitch angle calculation.

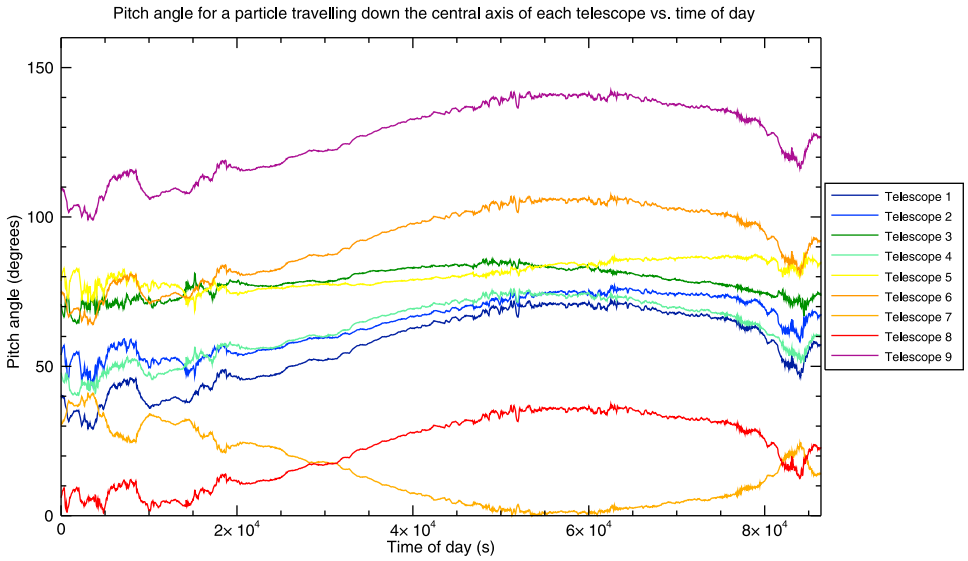


**Figure 2.** The pitch angle for a particle traveling down the central axis of each of the 9 telescopes of GOES-13 across a single day (09/11/2011).

frame of the spacecraft that changes in satellite attitude/orientation do not impact the computation of pitch angles. Distortions which change the orientation of a telescope relative to the magnetometer, such as thermally induced changes in the orientation of the magnetometer boom relative to the spacecraft body while on orbit, have potential to impact the pitch angles determined and therefore increase the uncertainty of the results. This particular uncertainty, however, is expected to be negligible relative to other uncertainties present in the data being analyzed.

[6] All detectors were assumed to have identical measurement characteristics initially, and therefore the data are initially processed using a single geometric factor derived from a pre-launch analysis (GOESN-ENG-048, 2011, http://www.ngdc.noaa.gov/stp/satellite/goes/doc/goes_nop/GOESN-ENG-048_RevD_EPS_HEPAD_13May2011.pdf).

[7] GOES-13 has two magnetometers. Each has three sensors oriented to within one degree of each spacecraft axis; their data are available at a 512 ms cadence. The accuracy of each magnetometer is 1 nT, with an expected 1 sigma RMS noise of 0.1 nT (GOES-N Data Book, 2005, http://goes.gsfc.nasa.gov/text/GOES-N_Databook/databook.pdf). On the recommendation of the Space Weather Prediction Center (SWPC), only data from Magnetometer 1 were used. Magnetometer 2 data for this satellite are strongly affected by noise caused by heater currents and require additional correction (H. Singer, private communication, 2011).

## 3. Method

[8] A representative pitch angle for particles entering each telescope was computed based on the dot product of the magnetic field vector (averaged over the telescope's integration period at the energy in question) with the vector opposite to the telescope's look direction. This yielded pitch angles which could range from 0 to 180 degrees. Pitch angles being sampled when the telescopes matched generally ranged between 20 and 120 degrees (e.g., Figure 2). If any of the magnetometer measurements were flagged because of a data quality issue or if the magnetometer was being calibrated, all data for that integration period were discarded.

[9] The data used in this study were obtained by identifying time intervals in which the pitch angle of particles entering along the central axis of the look direction for two telescopes matched to within one degree, similar to the approach by (T. Onsager, unpublished material, 2006) during post-launch test. The data include the count rate measured by each telescope for every integration cycle of each energy channel during matching time intervals. Any data for which these pitch angles were changing quickly (at a rate greater than 1 degree per integration cycle) were eliminated, which decreased the standard deviation of the results by approximately a factor of two in the low count rate data.

[10] The matched data from each telescope pair with nonzero number of matches was used to determine a correction scale factor using a minimization technique. For a given energy channel, an initial correction scale factor, *SF*, of 1.0 was assumed for each of the nine telescopes and the relative difference $R(m)$ between telescopes $i$ and $j$ for match $m$

$$\mathrm{R(m)} = \frac{\mathrm{SF_i CR_i(m)} - \mathrm{SF_j CR_j(m)}}{\mathrm{SF_i CR_i(m)} + \mathrm{SF_j CR_j(m)}}$$

for $i \neq j$ was computed for all matched count rates, $CR(m)$, for all telescope pairs with nonzero matches. The sum of the square of the relative differences for all matches was used as the objective quantity to be minimized with

**Table 3.** Results From Proxy Data Testing

| | Number of Matches for a Given Pair of Telescopes | | | Geometric Factor (GF) of Instrument | | |
|---|---|---|---|---|---|---|
| | T1-T2 | T1-T3 | T2-T3 | T1 | T2 | T3 |
| Case 1 | 100000 | 100000 | 100000 | 1.0 | 1.0 | 1.0 |
| Case 2 | 1000 | 100000 | 100000 | 1.0 | 1.0 | 0.5 |
| Case 3 | 100000 | 100000 | 1000 | 1.0 | 1.0 | 0.5 |
| Case 4 | 100000 | 100000 | 100000 | 1.2 | 1.0 | 0.8 |
| Case 5 | 100000 | 10 | 100000 | 1.1 | 1.0 | 0.9 |
| | Scale Factor (SF) Analysis Result | | | Result of SF*GF | | |
| | T1 | T2 | T3 | T1 | T2 | T3 |
| Case 1 | 1.01 | 1.01 | 1.01 | 1.01 | 1.01 | 1.01 |
| Case 2 | 0.75 | 0.74 | 1.49 | 0.75 | 0.74 | 0.75 |
| Case 3 | 0.75 | 0.75 | 1.51 | 0.75 | 0.75 | 0.76 |
| Case 4 | 0.80 | 0.96 | 1.20 | 0.96 | 0.96 | 0.96 |
| Case 5 | 0.91 | 1.00 | 1.11 | 1.00 | 1.00 | 1.00 |

respect to the nine scale factors. This minimization procedure was performed individually upon each energy band to permit determination of whether the results might be a function of energy. (Thickening of the dead layer of an SSD, for example, could affect the count rate of the lowest energy channels while leaving the upper energy channels relatively untouched, depending on the logic being used in the instrument.)

[11] A relative difference was selected instead of an absolute difference because the geometric factor derived should apply equally to data across the measurement range of the instrument. If the absolute difference were selected, it would give more weight to the highest count rates.

[12] The counts measured per integration cycle by these instruments are expected to follow a Poisson distribution for low count rates, which introduces a relative uncertainty equal to $\frac{1}{\sqrt{N_c}}$, where $N_c$ is the number of counts collected in the integration cycle. This means that the data which were taken with fewer counts in an integration cycle have higher statistical relative uncertainty, for example if the detector counted 10000 counts in an integration cycle the expected Poisson relative uncertainty is 1%, for 1000 counts it is on the order of 3%, and for 100 counts it is 10%. The true total relative uncertainty of the GOES measurements from each telescope was not known a priori, and would depend upon the amount of contamination present for any given measurement. However, the requirement for the relative uncertainty of the channel thresholds is 15%, as is the requirement for temperature stability of these thresholds. Additional terms beyond the threshold uncertainties would contribute to the uncertainty in the instrument response. It is therefore expected that the total uncertainty in the instrument response is greater than 15%. In order to determine whether the additional dynamic uncertainty from Poisson statistics had a substantial impact on our results, calculations were performed both with the full data set and with only the data having more than 1000 counts per integration cycle. In this second data subset even the counting statistics for the lowest count rates present correspond to a relative uncertainty on the order of 3%, which should be negligible relative to the total uncertainty as well as the other dynamic uncertainties in the instruments.

[13] The minimization was performed using an unconstrained Nelder-Mead algorithm, [*Fausett*, 1999] with a tolerance on the scale factor of 0.001 and a tolerance on the objective quantity of 0.0001. To test whether the result depended on the initial scale factors, 30 trials using the Nelder-Mead technique (as implemented in the MATLAB version 7.10.0 *fminsearch function*) were performed using initial scale factors normally distributed about 1.0 with a standard deviation of 0.2 (Tables 11a and 11b and Table 12 and the discussion of these tables). To determine if the solution depended on the minimization method, ten trials using the Quasi-Newton line search method [Press *et al.*, 2007] (as implemented in the MATLAB version 7.10.0 *fminunc function*) were performed. These trials also used randomized starting scale factors. In both cases, the results were statistically consistent with the Nelder-Mead results and bootstrap estimated uncertainty.

[14] Because this implementation is solely an intracalibration, no external values (or additional satellite data) were used to constrain the scale factor results. Minimization of the objective quantity could, therefore, give a significantly different scale factor for a given telescope even if that telescope has not actually changed in an absolute sense, but only relative to one or more other telescopes. Consider a scenario in which this procedure is applied to an instrument which only has three telescopes, $T_1$, $T_2$, and $T_3$. Suppose that all three telescopes begin operations with identical geometric factors. The algorithm finds that the best scale factor is statistically equal for each telescope. After the first year of operations, a $T_3$'s response is reduced by 50%, while $T_1$ and $T_2$ do not degrade at all. The solution given by the algorithm could be anything along the line $SF_{T3} = 2*SF_{T1,2,}$ with results including the scale factors of 0.75 for $T_1$ and $T_2$, and 1.5 for $T_3$. Table 3 gives results for an analysis of proxy data under various conditions. The Box-Muller [*Box and Muller*, 1958] method for generating normally distributed random numbers was used during proxy data generation to introduce a relative standard deviation of 25% into the count rate data for each telescope. The intracalibration method successfully corrects the results of the telescopes relative to one another, but an additional constraint is needed to produce results that are correct in an absolute sense. This constraint could come from a priori knowledge of the environment or from intercalibration with additional satellites.

[15] Although the uncertainties in the mounting of the magnetometer instruments are known (GOES-N Data Book, 2005, http://goes.gsfc.nasa.gov/text/GOES-N_Databook/databook.pdf), the mounting uncertainties for the MAGED telescopes are not available. For this reason it is

**Table 4.** Number of Data Points for Comparisons Between Telescopes for the 30–50 keV Energy Range With Count Rates per Integration Cycle Greater Than Zero and Change in Pitch Angle Less Than 1 Degree per Integration Cycle

| Telescope | 2 | 3 | 4 | 5 | 6 | 7 | 8 | 9 |
|---|---|---|---|---|---|---|---|---|
| 1 | 43076 | 831 | 142087 | 42 | 0 | 6760 | 0 | 0 |
| 2 | | 35939 | 1244433 | 2 | 38 | 3173 | 0 | 0 |
| 3 | | | 0 | 797014 | 23420 | 24 | 2 | 0 |
| 4 | | | | 10103 | 0 | 3624 | 26 | 0 |
| 5 | | | | | 42538 | 0 | 0 | 26 |
| 6 | | | | | | 0 | 0 | 0 |
| 7 | | | | | | | 79369 | 0 |
| 8 | | | | | | | | 0 |

**Table 6.** Standard Deviation of Relative Difference for the 30–50 keV Channel With Count Rates per Integration Cycle Greater Than Zero and Change in Pitch Angle Less Than 1 Degree per Integration Cycle

| Telescope | 2 | 3 | 4 | 5 | 6 | 7 | 8 | 9 |
|---|---|---|---|---|---|---|---|---|
| 1 | 0.033 | 0.099 | 0.033 | 0.052 | 0 | 0.12 | 0 | 0 |
| 2 | | 0.045 | 0.040 | 0.12 | 0.46 | 0.15 | 0 | 0 |
| 3 | | | 0 | 0.054 | 0.12 | 0.23 | 0.31 | 0 |
| 4 | | | | 0.054 | 0 | 0.16 | 0.25 | 0 |
| 5 | | | | | 0.16 | 0 | 0 | 0.29 |
| 6 | | | | | | 0 | 0 | 0 |
| 7 | | | | | | | 0.058 | 0 |
| 8 | | | | | | | | 0 |

not possible to directly estimate the pitch angle uncertainty. Instead, the uncertainties on the computed correction factors were calculated using a bootstrap re-sampling approach [*Efron and Tibshirani*, 1993]. Fifty sets of nine scale factors were computed using a random sample (with replacement) of one-half of the matches. This permitted determination of the standard deviation of the scale factors computed using all of the matches. So long as sufficient matches exist to ensure that a representative sample is present for a given telescope, this technique gives a statistically valid result for the uncertainty in the scale factor. Results should not be used when the total number of matches for a given telescope is small. A possible cutoff would be when the number of matches for a given telescope is less than 30 [*Chernick*, 2008]. Examining the total number of matches for each telescope using Table 4 shows that there might be too few matches in the 30 keV to 50 keV channel for Telescope 9's scale factors (the higher energy channels, which have a smaller number of matches, are likely to be more problematic), but that it should not be an issue for the other telescopes in the 30–50 keV energy channel. The authors note that in the testing conducted in Tables 11a and 11b and Table 12, telescope 9 had a total number of matches on the order of 30 but the range in scale factors obtained varied by a factor of 3 during the randomized trials. We recommend that before applying a result, especially in systems with a large number of degrees of freedom, that results for each given telescope scale factor should be evaluated based both upon the number of matches that telescope had and upon the number of other scale factors that the solution was connected to. In this case T9 was only related to T5, and gave results which were clearly inconsistent while having on the order of 30 matches.

**Table 5.** Mean of Relative Difference $(CR_i - CR_j)/((CR_i + CR_j)/2)$ for the 30–50kev Channel With Count Rates per Integration Cycle Greater Than Zero and Change in Pitch Angle Less Than 1 Degree per Integration Cycle

| Telescope | 2 | 3 | 4 | 5 | 6 | 7 | 8 | 9 |
|---|---|---|---|---|---|---|---|---|
| 1 | −0.0976 | −0.0518 | −0.0492 | 0.0556 | 0 | −0.0435 | 0 | 0 |
| 2 | | 0.0556 | 0.0478 | 0.114 | 0.0545 | 0.0976 | 0 | 0 |
| 3 | | | 0 | 0.0492 | −0.0556 | −0.0479 | −0.372 | 0 |
| 4 | | | | 0.0478 | 0 | 0 | −0.126 | 0 |
| 5 | | | | | −0.0588 | 0 | 0 | −0.113 |
| 6 | | | | | | 0 | 0 | 0 |
| 7 | | | | | | | 0 | 0 |
| 8 | | | | | | | | 0 |

## 4. Results

[16] The data analyzed span the time period between May 4, 2010 and Sept. 31, 2010. These constitute the first several months after the launch of GOES-13. Statistics of the results for the 30–50 keV channel are summarized in Tables 4, 5, and 6. Some telescopes routinely return count rates higher or lower than others. The fact that certain matches do not occur frequently for this three-axis-stabilized satellite increases the uncertainty in the task of finding changes to the geometric factors for some telescopes, such as Telescope 9.

[17] Another effect which was considered is excessive dead-time in one telescope relative to the others. A diagnostic for this would be a significant change in the percent difference between telescopes as a function of count rate. An electronics issue or a noisy detector incessantly triggering the lowest energy threshold within the detector can trigger this sort of effect in detectors which require the lowest energy threshold to be in anticoincidence with other thresholds to identify a count (veto logic). The MAGED does not incorporate veto logic for the lowest threshold values (Tables 7a and 7b), therefore if such an

**Table 7a.** MAGED Thresholds (GOESN-ENG-048)[a]

| Threshold Level Number | Threshold Value (keV) |
|---|---|
| 1 | 25.6 |
| 2 | 47.0 |
| 3 | 98.0 |
| 4 | 199.0 |
| 5 | 349.0 |
| 6 | 599.0 |

[a]Table 7a gives energy values that will trigger the various threshold levels of the detector when met.

**Table 7b.** MAGED Coincidence Logic and Energy Range (GOESN-ENG-048)[a]

| Channel Designation | Coincidence Logic | Energy Range (keV) |
|---|---|---|
| ME1 | 1 * $\overline{2}$[b] | 30 to 50 |
| ME2 | 1 * $\overline{2}$ * 3 | 50 to 100 |
| ME3 | 1 * 3 * $\overline{4}$ | 100 to 200 |
| ME4 | 1 * 4 * $\overline{5}$ | 200 to 350 |
| ME5 | 1 * 5 * $\overline{6}$ | 350 to 600 |

[a]Table 7b gives the nominal energy ranges of the energy channels, and the coincidence logic required (what combination of the thresholds listed in Table 7a must be triggered) to constitute a count. This means that for a count to be measured in the 50 keV to 100 keV channel that at least 47.0 keV of energy must be measured by the detector, but no more than 98.0 keV can be detected within a very short window. (Based on the range of count rates measurable by the instrument, a value in the range of microseconds would be expected.) The detector threshold levels are, in general, not the same as the boundaries of an energy level for a particle detector. In cases where the particle stops, as is the case for these relatively low energy electrons, they are fairly close, with some discrepancy due to effects such as energy being lost in non-active parts of the detector (e.g., dead layer). For particles which do not stop in the detector (or for energy deposited in a single detector from a multidetector instrument such as the MAGPD) the energy deposited can be substantially less than the particle energy, and the coincidence logic can become much more complicated. Additionally, the amount of energy deposited by a given non-stopping particle depends upon the angle at which it passes through the detector, as this affects the amount of detector material that the particle passes through on its journey. The modeled Particle Energy versus Energy Lost in Detector for the GOES-N series MAGED detectors is available in vendor documentation (GOES-N ENG-048, Figure 4–4). In general, the appropriate thresholds and coincidence logic are estimated during the design phase by using models of the energy which will be deposited in the detector for a given particle energy and type. The response of one or more telescopes is, generally speaking, subsequently testing during a ground calibration using particle sources with known output spectra and flux. Often this utilizes the output available at a particle-beam facility. In the case of the MAGED, ground calibration included measurements at multiple accelerators. The geometric factors of the instrument for particles of various energies that were determined based upon these calibrations are specified in GOESN-ENG-048.

[b]1 * 2 is read as "level 1 but not level 2."

issue occurs with this instrument the mechanism should be different. Figure 3 shows representative comparisons of the relative difference in two channels versus the count rate of a telescope. In this figure differences in the background detected by one telescope versus the other, being an additive effect, would be expected to have the largest impact at the lower count rates; a difference in the dead time of the telescopes would have a multiplicative effect at higher count rates. Qualitatively, the relative difference is centered about the same value across the range of available count rate data, which implies that these telescopes do not currently suffer from differing amounts of these issues. For such an issue to be apparent from the figure it would need to be sufficiently large to shift the central count rate results of the telescope by at least one step of the compression algorithm, i.e., 5% or larger. A more extensive analysis using a larger GOES MAGED data set should permit a quantitative assessment, and will be included in future work applying this intracalibration technique.

[18] Table 8 shows the scale factors computed using all data. Uncertainty was estimated using the bootstrapping technique described in section 3. Table 9 compares the computed scale factors when all matches were used to the averages obtained using 50 random samples of half of the data set. To determine if the observed scale factors are statistically different from 1.0, a one-sided t-test was performed using the 50 bootstrap values. In all cases, the null hypothesis that the observed scale factor came from a distribution with a mean of 1.0 can be rejected at the 1% significance level, except for the scale factor for Telescope 9. Table 10 shows the result following the same analysis for that of Table 9 when only matches for which the count rate was greater than 1000 cps were used.

[19] Performing the same analysis using the full data set across all energy bands yielded results showing that Telescopes 2 and 6 are consistently high. Many of the other telescopes that could require relatively small corrections yielded results that are inconsistent across the energy

**Figure 3.** Comparisons of relative percent difference between two telescopes versus the average of the telescopes' count rates for three telescope pair combinations. The irregularly shaped banding of the percent differences and large number of superimposed points result from the data compression algorithm (GOESN-ENG-048) used for the instrument. (a) Percent difference versus count rate for Telescopes 2 and 4 of the GOES-13 MAGED, 30–50 keV energy bin, for data spanning the range from May 4, 2010 to September 30, 2010. Data plotted are those for which the pitch angles for the two telescopes matched to within 1 degree. Data were further screened to ensure that only data with a change in pitch angle of less than 1 degree per integration cycle appear. Data compression often causes the same position on the plot to represent more than one match of pitch angle. Because of this, a logarithmic color scale was used to denote the number of instances of each data point. In this plot, black begins at 1 instance, blue at 154 instances, and red at 23706 instances. (b) Percent difference versus count rate for Telescopes 3 and 5 of the GOES-13 MAGED, 30–50 keV energy bin, for data spanning the range from May 4, 2010 to September 30, 2010. Data plotted are those for which the pitch angles for the two telescopes matched to within 1 degree. Data were further screened to ensure that only data with a change in pitch angle of less than 1 degree per integration cycle appear. In this plot, black begins at 1 instance, blue at 108 instances, and red at 11619 instances. (c) Percent difference versus count rate for Telescopes 2 and 3 of the GOES-13 MAGED, 30–50 keV energy bin, for data spanning the range from May 6, 2010 to September 27, 2010. The same date range of data were input to the algorithms as in Figures 3a and 3b, but data meeting the matching criteria fell within this shorter date range. In this plot, black begins at 1 instance, blue at 34 instances, and red at 1146 instances.

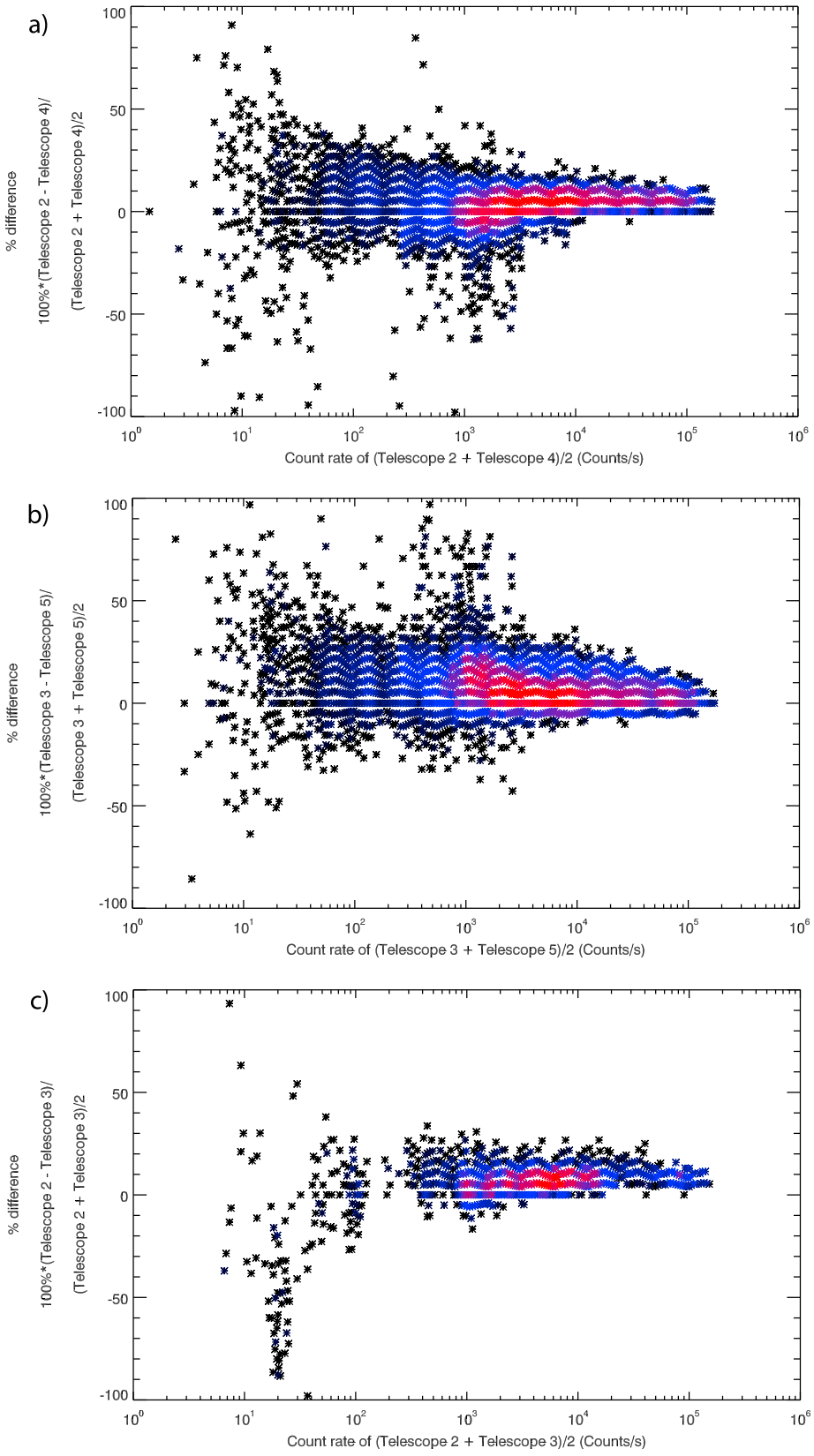
a)
% difference
100%*(Telescope 2 - Telescope 4)/
(Telescope 2 + Telescope 4)/2
Count rate of (Telescope 2 + Telescope 4)/2 (Counts/s)
b)
% difference
100%*(Telescope 3 - Telescope 5)/
(Telescope 3 + Telescope 5)/2
Count rate of (Telescope 3 + Telescope 5)/2 (Counts/s)
c)
% difference
100%*(Telescope 2 - Telescope 3)/
(Telescope 2 + Telescope 3)/2
Count rate of (Telescope 2 + Telescope 3)/2 (Counts/s)

**Figure 3**

**Table 8.** Comparison of Results for the Full Data Set, Count Rates >0, for All Energy Channels and Telescopes

| Telescope | 30–50 (keV) | 50–100 (keV) | 100–200 (keV) | 200–350 (keV) | 350–600 (keV) |
|---|---|---|---|---|---|
| 1 | 1.035 | 1.010 | 1.017 | 1.043 | 0.965 |
| 2 | 0.950 | 0.952 | 0.969 | 0.965 | 0.977 |
| 3 | 1.011 | 1.003 | 0.996 | 0.989 | 0.986 |
| 4 | 0.987 | 0.999 | 1.011 | 1.034 | 1.032 |
| 5 | 1.064 | 1.033 | 1.019 | 0.999 | 1.000 |
| 6 | 0.940 | 0.954 | 0.955 | 0.967 | 0.940 |
| 7 | 1.010 | 1.001 | 0.986 | 0.980 | 0.999 |
| 8 | 1.018 | 1.037 | 1.040 | 1.051 | 1.073 |
| 9 | 1.004 | 1.020 | 1.022 | 0.982 | 1.065 |

**Table 10.** Comparison of Full Data Set Results to Bootstrap Results Using Only Matches With Count Rate >1000 cps for the 30–50 keV Channel

| Telescope | Scale Factor | Average of 50 Scale Factors | STD of 50 Scale Factors |
|---|---|---|---|
| 1 | 1.0433 | 1.0397 | 0.0050 |
| 2 | 0.9580 | 0.9547 | 0.0046 |
| 3 | 1.0198 | 1.0163 | 0.0048 |
| 4 | 0.9953 | 0.9917 | 0.0048 |
| 5 | 1.0724 | 1.0687 | 0.0051 |
| 6 | 0.9735 | 0.9702 | 0.0047 |
| 7 | 1.0169 | 1.0129 | 0.0050 |
| 8 | 1.0239 | 1.0200 | 0.0050 |
| 9 | 0.9345 | 0.9638 | 0.0299 |

range. The lack of valid matches over the time period examined makes it impossible to derive suitable scale factors in some cases, especially for Telescope 9. Extending the data set could provide the information necessary to obtain consistent corrections for these telescopes. This would be especially helpful in the higher energy channels, as their longer integration period results in a much lower frequency of valid matches (Table 2 versus Table 4).

[20] During disturbed periods, situations can occur where the first adiabatic invariant may be violated [e.g., *Li et al.*, 1999]. To determine whether this influenced the intracalibration results, a data set was generated which used the epoch of each pitch angle match to correlate it to the Dst value at that time. The values for the disturbed time periods did not appear to be correlated to the most extreme relative differences in the data set, indeed they generally appeared to be correlated with relative differences near the average values. If most values from the telescopes are distributed about some average relative difference then this is expected, as sampling the distribution should also yield points that are similarly distributed about the same average value.

[21] Determination of whether the computed scale factors are actually a local minimum for the objective function rather than a global minimum is another potential problem. In the case of the results presented, a limited set of runs was performed in which the starting scale factors used were randomized. Specifically, 30 runs were performed using scale factors normally distributed about 1.0 with a standard deviation of 0.2. If a better minimum was present, this could permit the algorithm to converge there in at least some of the trials. The results from 10 of these trials will be displayed here, but results were consistent across the set. The earlier discussion concerning the fact that only a relative intracalibration can be obtained based on the data available is extremely pertinent. The randomized initial scale factors for 10 trials are listed in Table 11a. A comparison of results with randomized initial scale factors to those with static ones (Table 11b), shows that while the absolute values of the solutions for the various channels do change as the initial scale factors are varied (which is expected, as discussed in section 3), the relative values of the scale factors are consistent with those determined using a starting scale factor of 1.0 for all telescopes. Table 11b shows this for ten of the trials by taking the ratio of each scale factor result to the result that was obtained using static initial scale factors. The ratio of the results obtained from data beginning with randomized scale factors to the results obtained from those beginning

**Table 9.** Comparison of Full Data Set Results to Bootstrap Results Using Only Matches With Count Rate >0 cps for the 30–50 keV Channel

| | Pitch Angle Derivative Not Constrained | | | Pitch Angle Derivative <1 Degree/Integration Cycle | | |
|---|---|---|---|---|---|---|
| Telescope | Scale Factor | Average of 50 Scale Factors | Standard Deviation of 50 Scale Factors | Scale Factor | Average of 50 Scale Factors | Standard Deviation of 50 Scale Factors |
| 1 | 1.0355 | 1.0368 | 0.0037 | 1.0348 | 1.0359 | 0.0019 |
| 2 | 0.9512 | 0.9524 | 0.0034 | 0.9504 | 0.9516 | 0.0017 |
| 3 | 1.0116 | 1.0128 | 0.0037 | 1.0106 | 1.0118 | 0.0020 |
| 4 | 0.9881 | 0.9893 | 0.0035 | 0.9873 | 0.9885 | 0.0018 |
| 5 | 1.0644 | 1.0658 | 0.0039 | 1.0635 | 1.0647 | 0.0021 |
| 6 | 0.9407 | 0.9417 | 0.0035 | 0.9397 | 0.9410 | 0.0018 |
| 7 | 1.0102 | 1.0117 | 0.0035 | 1.0100 | 1.0113 | 0.0019 |
| 8 | 1.0186 | 1.0201 | 0.0035 | 1.0184 | 1.0197 | 0.0019 |
| 9 | 1.0036 | 0.9883 | 0.0290 | 1.0040 | 0.9957 | 0.0157 |

**Table 11a.** Randomized Initial Scale Factors for Each Telescope Generated in 10 Separate Trials, to Determine What Impact These Had Upon the Final Results

| | Randomized Initial SF Values | | | | | | | | | |
|---|---|---|---|---|---|---|---|---|---|---|
| | Trial 1 | Trial 2 | Trial 3 | Trial 4 | Trial 5 | Trial 6 | Trial 7 | Trial 8 | Trial 9 | Trial 10 |
| SF1i | 1.3424 | 0.6078 | 1.2197 | 1.0067 | 0.8337 | 0.8404 | 0.7760 | 0.5340 | 0.7277 | 0.9864 |
| SF2i | 0.9612 | 0.9605 | 0.9444 | 0.7333 | 0.8042 | 1.2037 | 1.5052 | 0.7102 | 1.0910 | 0.9610 |
| SF3i | 0.5723 | 0.7584 | 1.1403 | 1.2255 | 0.7687 | 0.9734 | 1.3311 | 1.0667 | 0.8303 | 0.9565 |
| SF4i | 0.8321 | 1.5816 | 0.5896 | 1.0700 | 0.8933 | 0.8571 | 1.0615 | 1.0783 | 0.9330 | 0.9394 |
| SF5i | 1.2709 | 1.1650 | 0.9292 | 0.9402 | 0.5995 | 1.2703 | 0.7486 | 1.0903 | 1.1106 | 1.0046 |
| SF6i | 0.7856 | 1.2758 | 0.8353 | 1.0046 | 1.1928 | 0.9550 | 0.8269 | 0.9739 | 1.2078 | 1.0103 |
| SF7i | 1.1922 | 0.7884 | 0.6846 | 0.9476 | 1.1040 | 0.8822 | 0.9647 | 1.0367 | 0.7765 | 1.1652 |
| SF8i | 1.0248 | 0.9063 | 1.1016 | 0.6500 | 0.9960 | 0.9412 | 1.1583 | 0.9048 | 1.2521 | 1.3054 |
| SF9i | 1.2873 | 0.9455 | 1.0564 | 0.9429 | 0.9930 | 0.8304 | 0.7336 | 1.1724 | 1.1320 | 1.0934 |

with no randomization is statistically the same for each telescope (except T9) in each trial, indicating that the scale factors obtained for each telescope are the same in a relative sense.

[22] Relative changes in the scale factors could also be demonstrated by taking the ratio of the scale factor obtained for each telescope in the randomized trials to that obtained for a "standard" telescope (Table 12). This second approach could be a helpful way to view the scale factor results in a case where a single telescope is expected to suffer very few changes over an extended period (or few changes relative to the other telescopes). It also produces a set of factors which are scaled consistently, which would be useful for comparisons of residuals from multiple solutions if multiple distinct solutions were found. In this case, Telescope 4 was used as the "standard" in Table 12 on the grounds that it has the largest number of matches, with significant numbers of matches spread across many of other telescopes. If a more complete analysis were to be performed then useful items to consider include both whether the physical properties of the telescope are expected to remain consistent for all of the comparisons in question and the statistics of the matches available for that telescope (total number of matches to the potential standard, number of telescopes with significant numbers of matches to the potential standard). It should be noted that T9 produced inconsistent results in this set of trials, which

**Table 11b.** Comparison of Results for 10 Trials With Randomized Initial Scale Factors to Those With a Static Initial Scale Factor[a]

| | Final SF Values Using Randomized Initial SF | | | | | | | | | | | |
|---|---|---|---|---|---|---|---|---|---|---|---|---|
| | Trial 1 | Trial 2 | Trial 3 | Trial 4 | Trial 5 | Trial 6 | Trial 7 | Trial 8 | Trial 9 | Trial 10 | SF Results With Static Initial SF | |
| SF1f | 0.9210 | 1.0123 | 0.9362 | 0.9823 | 0.9840 | 1.0152 | 1.0236 | 0.9143 | 1.0420 | 1.1074 | SF1static | 1.0355 |
| SF2f | 0.8461 | 0.9299 | 0.8600 | 0.9024 | 0.9039 | 0.9326 | 0.9403 | 0.8399 | 0.9572 | 1.0173 | SF2static | 0.9512 |
| SF3f | 0.8995 | 0.9888 | 0.9144 | 0.9590 | 0.9612 | 0.9917 | 0.9998 | 0.8933 | 1.0179 | 1.0817 | SF3static | 1.0116 |
| SF4f | 0.8789 | 0.9659 | 0.8933 | 0.9373 | 0.9389 | 0.9687 | 0.9767 | 0.8724 | 0.9943 | 1.0567 | SF4static | 0.9881 |
| SF5f | 0.9466 | 1.0405 | 0.9622 | 1.0091 | 1.0115 | 1.0436 | 1.0521 | 0.9400 | 1.0711 | 1.1382 | SF5static | 1.0644 |
| SF6f | 0.8362 | 0.9195 | 0.8502 | 0.8918 | 0.8939 | 0.9223 | 0.9298 | 0.8306 | 0.9466 | 1.0059 | SF6static | 0.9407 |
| SF7f | 0.8990 | 0.9875 | 0.9136 | 0.9584 | 0.9600 | 0.9905 | 0.9987 | 0.8919 | 1.0166 | 1.0808 | SF7static | 1.0102 |
| SF8f | 0.9063 | 0.9957 | 0.9212 | 0.9660 | 0.9679 | 0.9987 | 1.0070 | 0.8993 | 1.0250 | 1.0898 | SF8static | 1.0186 |
| SF9f | 1.9593 | 1.0164 | 1.0204 | 0.6217 | 0.9065 | 0.7855 | 0.7425 | 1.0200 | 0.9601 | 0.8898 | SF9static | 1.0036 |
| | Ratio of Final SF for Each Channel to That Obtained Using Static Initial Scale Factors | | | | | | | | | | | |
| | Trial 1 | Trial 2 | Trial 3 | Trial 4 | Trial 5 | Trial 6 | Trial 7 | Trial 8 | Trial 9 | Trial 10 | | |
| SF1f/SF1static | 0.8895 | 0.9776 | 0.9041 | 0.9486 | 0.9503 | 0.9804 | 0.9885 | 0.8830 | 1.0063 | 1.0695 | | |
| SF2f/SF2static | 0.8896 | 0.9777 | 0.9041 | 0.9487 | 0.9503 | 0.9805 | 0.9886 | 0.8830 | 1.0063 | 1.0695 | | |
| SF3f/SF3static | 0.8892 | 0.9775 | 0.9039 | 0.9480 | 0.9502 | 0.9804 | 0.9884 | 0.8830 | 1.0062 | 1.0693 | | |
| SF4f/SF4static | 0.8895 | 0.9776 | 0.9041 | 0.9486 | 0.9502 | 0.9804 | 0.9885 | 0.8829 | 1.0063 | 1.0694 | | |
| SF5f/SF5static | 0.8893 | 0.9775 | 0.9040 | 0.9481 | 0.9503 | 0.9804 | 0.9885 | 0.8831 | 1.0063 | 1.0694 | | |
| SF6f/SF6static | 0.8890 | 0.9775 | 0.9038 | 0.9480 | 0.9502 | 0.9804 | 0.9884 | 0.8830 | 1.0062 | 1.0693 | | |
| SF7f/SF7static | 0.8899 | 0.9776 | 0.9044 | 0.9487 | 0.9503 | 0.9805 | 0.9886 | 0.8829 | 1.0063 | 1.0699 | | |
| SF8f/SF8static | 0.8898 | 0.9775 | 0.9043 | 0.9484 | 0.9502 | 0.9804 | 0.9886 | 0.8829 | 1.0062 | 1.0699 | | |
| SF9f/SF9static | 1.9523 | 1.0127 | 1.0167 | 0.6194 | 0.9033 | 0.7827 | 0.7398 | 1.0164 | 0.9566 | 0.8866 | | |

[a]Data used were 30–50 keV channel, all matches with CR > 0, pitch angle derivative unconstrained (constituting the largest single data set available).

**Table 12.** Comparison of Results for 10 Trials With Randomized Initial Scale Factors to the Scale Factor for a Selected "Standard" Telescope (T4)[a]

| | Ratio of Final SF to a "Standard" Telescope's (T4) Final SF | | | | | | | | | |
|---|---|---|---|---|---|---|---|---|---|---|
| | Trial 1 | Trial 2 | Trial 3 | Trial 4 | Trial 5 | Trial 6 | Trial 7 | Trial 8 | Trial 9 | Trial 10 |
| SF1f/SF4f | 1.0480 | 1.0480 | 1.0480 | 1.0480 | 1.0480 | 1.0480 | 1.0480 | 1.0480 | 1.0480 | 1.0480 |
| SF2f/SF4f | 0.9627 | 0.9627 | 0.9627 | 0.9627 | 0.9627 | 0.9627 | 0.9628 | 0.9627 | 0.9627 | 0.9627 |
| SF3f/SF4f | 1.0235 | 1.0237 | 1.0236 | 1.0231 | 1.0238 | 1.0237 | 1.0237 | 1.0239 | 1.0237 | 1.0236 |
| SF4f/SF4f | 1.0000 | 1.0000 | 1.0000 | 1.0000 | 1.0000 | 1.0000 | 1.0000 | 1.0000 | 1.0000 | 1.0000 |
| SF5f/SF4f | 1.0770 | 1.0772 | 1.0771 | 1.0766 | 1.0773 | 1.0773 | 1.0772 | 1.0774 | 1.0773 | 1.0772 |
| SF6f/SF4f | 0.9515 | 0.9519 | 0.9518 | 0.9515 | 0.9520 | 0.9520 | 0.9520 | 0.9521 | 0.9520 | 0.9519 |
| SF7f/SF4f | 1.0228 | 1.0224 | 1.0227 | 1.0225 | 1.0224 | 1.0224 | 1.0226 | 1.0224 | 1.0224 | 1.0228 |
| SF8f/SF4f | 1.0312 | 1.0308 | 1.0312 | 1.0306 | 1.0308 | 1.0309 | 1.0310 | 1.0308 | 1.0309 | 1.0313 |
| SF9f/SF4f | 2.2293 | 1.0522 | 1.1422 | 0.6632 | 0.9655 | 0.8108 | 0.7602 | 1.1692 | 0.9656 | 0.8420 |

is consistent with our assertion that results for telescopes with very small numbers of matches should not be trusted.

[23] An extension of the analysis to include data from the equivalent (May through Sept.) time interval of 2011 yielded the results listed in Table 13. For most telescopes the results do not appear to have changed significantly. Telescope 8 is an exception. Based on the 2010 statistics, this telescope's 2011 scale factor is 40 standard deviations from the one calculated using the 2010 data. This demonstrates that this particular telescope had its count rate increase relative to the other telescopes. The reason for this could be that the other telescopes' count rates decreased while telescope 8's decreased somewhat more slowly, or that its count rate has increased substantially relative to the others. This shift was detected in both the low and high energy channels. A detailed analysis seeking a probable root cause is beyond the scope of this paper.

## 5. Discussion

[24] One application of the technique discussed and used in this paper could be a regularly updated multiplicative scaling factor that can be applied to each telescope. Normalization of these factors could be performed to permit continuity of data, or additional knowledge from inter-calibration with other satellites or the environment (meaning periods of time during which confidence exists that another instrument on a different satellite should be returning the same values, or that the expected particle flux distribution is known) could be used. Comparison of response changes between energy channels could permit identification of degradation in the instrument itself, due to, for example, thickening of the dead layer of an SSD via introduction of lattice defects. These defects trap electrons and holes that are formed by the particle passing through the detector. If the electrons and holes are trapped for a sufficiently long amount of time they can be missed by the detector logic. When these defects occur near the surface this can effectively increase the "dead layer" of the detector. When in the bulk, these defects can be associated with an effective decrease in bias voltage (potentially compensated for by setting a higher bias voltage) and increase in detector leakage current, increasing noise in the lowest energy channels [*Wüest et al.*, 2007].

[25] This method should also be applicable to inter-calibration with detectors at LEO. To accomplish such an inter-calibration, first a successful intracalibration of each instrument must be performed. This must include making certain that no gross calibration errors exist in the energy responses of the candidate satellites. The next step would be to find periods in which the particles measured by the satellites should be traveling along the same field line. Once a candidate time period is identified, one could determine whether the spectral shape measured by the satellites agree. If the spectra do not agree, it could indicate that magnetic conjugacy did not occur during that time interval [*Reeves et al.*, 1996]. A comparison of the magnetic field measured by each satellite versus that predicted by the model would be a second useful screening parameter.

**Table 13.** Results for Analysis From May Through September 2010 Versus 2011, 30–50 keV Channel

| Telescope | 2010 | 2011 | 2010 CR > 1000 | 2011 CR > 1000 | 2011, DTC | 2011, DTC CR > 1000 |
|---|---|---|---|---|---|---|
| 1 | 1.04 | 1.03 | 1.04 | 1.04 | 1.04 | 1.05 |
| 2 | 0.95 | 0.95 | 0.95 | 0.96 | 0.95 | 0.96 |
| 3 | 1.01 | 1.03 | 1.02 | 1.04 | 1.03 | 1.04 |
| 4 | 0.99 | 0.99 | 0.99 | 1.00 | 0.99 | 1.01 |
| 5 | 1.06 | 1.07 | 1.07 | 1.08 | 1.07 | 1.09 |
| 6 | 0.94 | 0.99 | 0.97 | 1.01 | 0.99 | 1.01 |
| 7 | 1.01 | 1.01 | 1.01 | 1.02 | 1.01 | 1.02 |
| 8 | 1.02 | 0.88 | 1.02 | 0.89 | 0.88 | 0.89 |
| 9 | 1.00 | 1.05 | 0.96 | 0.96 | 1.05 | 1.00 |

If the energy spectra and magnetic field comparisons show good agreement, then the analysis would proceed by calculation of the pitch angles corresponding to identical first adiabatic invariants for particles measured by each satellite. If any of the telescope pairs fall within this range, the data are saved and compared. Over time, a record can be established for various GEO-LEO pairs of telescopes, similar to the ones created here for telescopes aboard a single satellite. Because a valid intracalibration of the satellites would precede such an effort, this would permit determination of an additional satellite to satellite adjustment factor, allowing creation of a consensus intercalibration between networks of on orbit detectors.

[26] In identifying candidates for this comparison, major issues include:

[27] 1. The energy ranges must overlap. If the energy ranges are not identical then the nominal response of one instrument must be convolved with the energy spectrum of the particles during the time interval in question to create a measurement covering the same energy range as that covered by the other instrument. This process adds to the uncertainty of the comparison;

[28] 2. Presence of a magnetometer on both satellites. Models could be used for one or both, but this currently would substantially increase uncertainties; and

[29] 3. Field of view for the telescopes should be narrow relative to the scale of any anisotropic effects. This must be true before calculating pitch angle based on the pointing of the telescopes' central axes can be meaningful.

## 6. Conclusions

[30] An algorithm for intracalibrating measurements from particle detectors aboard three-axis stabilized satellites was described and analyzed. GOES-13 MAGED particle detector data were used, and scale factors were computed for each telescope; these scale factors may be used to correct for on-orbit changes to the instrument. For the 2010 data, the computed scale factors were generally on the order of 5%. This demonstrates that the technique is sensitive enough to detect and correct these systematic relative changes to obtain an internally consistent data set at a given time. It was also found that screening for rapid changes of the magnetic field reduced uncertainty in the computed scale factors. If the average geometric factor for the telescopes was equivalent to the nominal pre-flight value, which cannot be tested without further constraints (such as inter-calibration) and a longer data record, a 5% variation in a scale factor could indicate that a single telescope had a geometric factor that deviated by as much as 5% away from the nominal value.

[31] Application of the method to data from both 2010 and 2011 appears to show a 10% shift in the response of one of the MAGED telescopes. Given that GOES particle detectors typically provide data for an operational lifetime on the order of 10 years, repeated shifts of this magnitude from year to year could degrade data quality substantially if uncorrected. Testing with a larger data set is required to quantify the actual impact over an instrument's lifetime, as this particular 10% change may be due to a one-time issue rather than part of a trend. With further testing, including application to a larger data set, the technique has potential to permit correction of the data set for instrumental changes throughout the lifetime of an instrument.

[32] This method should be applicable to telescopes of particle detectors aboard other satellites that also carry a magnetometer. A magnetic field model could be used in lieu of a magnetometer, with the caveat that it could cause an increase in uncertainty that may limit the utility of the results, depending upon the needs of the program in question. Automating this analysis could provide a useful data record for the scientists responsible for maintaining accuracy of data from these instruments as well as the user community at large.

[33] The method should also be extensible to intercalibration between sensors located at Geostationary and Low-Earth Orbits, provided that suitable satellites having particle detectors with overlapping energy ranges and accurate magnetic field measurements at the satellite location are available. Such an activity could permit consistent (relative) accuracy of particle measurements at GEO and LEO altitudes, as well as between them.

[34] Discussion is underway with NOAA's National Geophysical Data Center (NGDC), Solar Terrestrial Physics (STP) Division to apply the software developed for this work to a larger data set that includes a longer time span and more satellites. If robustness and utility are demonstrated, this could lead to operational application of the software used in this analysis for the upcoming GOES-R series and maintenance of a publicly accessible record of calibration changes. Future work may also extend the technique to inter-calibration between different satellites, for example GEO-LEO comparisons, if suitable LEO platforms are available.

[35] The match data and the analysis code used for this work are available from VIRBO at ftp://virbo.org/users/rowland/pik and http://virbo.org/svn/rowland/pik, respectively.

[36] **Acknowledgments.** The authors gratefully acknowledge the efforts of Terry Onsager (SWPC), whose work was a progenitor for this effort. They also thank Juan Rodriguez (CIRES, SWPC, and NGDC), Janet Green (NGDC), and Howard Singer (SWPC) for many helpful conversations. The authors thank the reviewers for helpful comments. This research was performed using data supplied by NOAA's National Geophysical Data Center (NGDC). Special thanks are given to Dan Wilkinson and Bill Denig who helped with data access. The work by WR was partially funded by the GOES-R Program Office. RSW and WR were supported by NSF grant 0457577: FDSS: Faculty Development in Space Weather Research: A Systems Perspective.

## References

Box, G. E. P., and M. E. Muller (1958), A note on the generation of random normal deviates, *Ann. Math. Stat.*, *29*(2), 610–611, doi:10.1214/aoms/1177706645.

Chen, Y., R. H. W. Friedel, G. D. Reeves, T. G. Onsager, and M. F. Thomsen (2005), Multisatellite determination of the relativistic

electron phase space density at geosynchronous orbit: Methodology and results during geomagnetically quiet times, *J. Geophys. Res.*, *110*, A10210, doi:10.1029/2004JA010895.

Chernick, M. R. (2008), *Bootstrap Methods: A Guide for Practitioners and Researchers*, John Wiley, Hoboken, N. J.

Efron, B., and R. J. Tibshirani (1993), *An Introduction to the Bootstrap*, Chapman and Hall, New York

Fausett, L. (1999), *Applied Numerical Analysis Using MATLAB*, Prentice Hall, Upper Saddle River, N. J.

Friedel, R. H. W., S. Bourdarie, and T. E. Cayton (2005), Intercalibration of magnetospheric energetic electron data, *Space Weather*, *3*, S09B04, doi:10.1029/2005SW000153.

Li, X., D. N. Baker, M. Teremin, T. E. Cayton, G. D. Reeves, R. S. Selesnick, J. B. Blake, G. Lu, S. G. Kanekal, and H. J. Singer (1999), Rapid enhancements of relativistic electrons deep in the magnetosphere during the May 15, 1997, magnetic storm, *J. Geophys. Res.*, *104*(A3), 4467–4476, doi:10.1029/1998JA900092.

Press, W. H., S. A. Teukolsky, V. T. Vetterling, and B. P. Flannery (2007), *Numerical Recipes 3rd Edition: The Art of Scientific Computing*, Cambridge Univ. Press, Cambridge, U. K.

Reeves, G. D., L. A. Weiss, M. F. Thomsen, and D. J. McComas (1996), A quantitative test of different magnetic field models using conjunctions between DMSP and geosynchronous orbit, in *Radiation Belts: Models and Standards*, *Geophys. Monogr. Ser.*, vol. 97, edited by J. F. Lemaire, D. Heynderickx, and D. N. Baker, pp. 167–172, AGU, Washington, D. C., doi:10.1029/GM097p0167

Wüest, M., D. S. Evans, and R. von Steigler (2007), Calibration of particle instruments in space physics, *Sci. Rep. SR-007*, Int. Space Sci. Inst., Bern.